TRENDS IN SCIENCES 2026; 23(4): 11611
https://doi.org/10.48048/tis.2026.11611 RESEARCH ARTICLE

Enhanced Mercury (Hg^{2+}) Adsorption from Aqueous Solutions Using Bentonite-Coconut Shell Monolith Composites

Darmadi[1], Mirna Rahmah Lubis[1,*], Adisalamun[1], and Muhammad Zaki[2]

[1]Department of Chemical Engineering, Fakultas Teknik, Universitas Syiah Kuala, Banda Aceh 23111, Indonesia
[2]Process Technology Laboratory, Faculty of Engineering, Universitas Syiah Kuala, Banda Aceh 23111, Indonesia

([*]Corresponding author's e-mail: mirna@che.usk.ac.id)

Received: 15 August 15 2025, Revised: 10 September 2025, Accepted: 10 October 2025, Published: 30 December 2025

Abstract

Mercury pollution from artisanal mining and industry poses severe environmental risks. This contamination can be addressed using a low-cost monolith adsorbent. Therefore, this study develops a sustainable bentonite-coconut shell monolith as a low-cost adsorbent for mercury (Hg^{2+}) removal. The monoliths were prepared using bentonite, coconut shell charcoal and molasses as a binder and subsequently activated physically and chemically using HNO_3 (0.5 N and 1 N). Characterized by Fourier Transform Infrared Spectroscopy (FTIR), Scanning Electron Microscopy (SEM), Brunauer–Emmett–Teller (BET) and X-ray Diffraction (XRD) confirmed the presence of functional groups, heterogeneous porous structure and the absence of mercury impurities in the raw materials. Adsorption investigations were conducted at Hg^{2+} concentrations of 2 - 8 mg/L to evaluate removal efficiency, kinetics, and isotherm behavior. Results showed that HNO_3 activation enhanced functionality and porosity, with 1 N HNO_3-treated monoliths achieving 7.23 mg/g capacity and 90.16% removal efficiency. Kinetic data fitted the pseudo-first-order model best ($R^2 = 0.997$), with intraparticle diffusion as a secondary mechanism. Isotherm analysis revealed that physically activated bentonite-coconut shell monolith followed the Freundlich model ($R^2 = 1.000$), whereas chemical activation shifted the behavior toward the Langmuir model ($R^2 = 0.999$). With a production cost of only \$0.76 - 1.36/kg, well below commercial activated carbon, the monolith offers an efficient, affordable and sustainable option for mercury remediation.

Keywords: Adsorption, Bentonite, Coconut shell, Mercury ion, Monolith

Introduction

Mercury pollution from artisanal gold mining is a persistent, highly toxic pollutant that bioaccumulates [1] and causes severe health effects [2], with illegal artisanal mining in Aceh, Indonesia elevating Hg^{2+} in water beyond regulatory limits [3]. Conventional treatments (activated carbon, ion exchange, electrochemical methods [4]) are effective but costly and unsuitable for rural settings, making adsorption a preferred alternative for its simplicity [5] and cost-effectiveness. Mercury (Hg^{2+}) was chosen as a priority contaminant because of its toxicity, persistence and tendency to bioaccumulate in aquatic organisms, eventually entering the human food chain. Even at trace concentrations, mercury can cause severe neurological, renal and developmental disorders, making it a high-priority pollutant according to the World Health Organization (WHO) and the U.S. Environmental Protection Agency (EPA) [6]. Compared to other heavy metals such as Cu^{2+} or Ni^{2+}, mercury is particularly challenging to remove from wastewater because of its multiple oxidation states [7] and strong tendency to form complexes with organic and inorganic ligands. Therefore, development of effective, low-cost and sustainable adsorbents for Hg^{2+} remediation remains a research priority. Monolithic adsorbents are highlighted as eco-friendly, mechanically stable and low-pressure drop [8] materials that overcome drawbacks of powdered adsorbents – such as recovery difficulties and higher cost – supporting their potential for sustainable Hg^{2+} remediation.

Various adsorbents such as activated carbon, clays and biochar have been widely studied for Hg^{2+} removal. Despite their effectiveness, these adsorbents are typically produced in powdered form, which complicates recovery after use and limits their large-scale application. No studies have yet reported the utilization of coconut shell in monolithic form for metal adsorption applications.

Bentonite and coconut shell offer complementary properties for developing low-cost, sustainable adsorbents. Coconut shell, an abundant carbon-rich waste, poses environmental risks if discarded but can be converted into activated carbon or biochar with proven high removal efficiencies exceeding 95% for metals like Cu^{2+}, Ni^{2+} and Cr^{3+}, often fitting Langmuir isotherms and pseudo-second-order kinetics [9]. Similarly, acid-activated and manganese-doped coconut shell charcoal achieved 56% removal of Cr(VI) and was also effective for Fe^{3+} uptake [10]. In other studies, activated coconut shell waste showed high adsorption capacities of ~4.57 mg/L for Cu^{2+}, confirming its applicability under optimal contact time of 180 min [11]. Furthermore, magnetic coconut biochar has been tested for Pb^{2+} removal with capacities of ~170 mg/g [12], while phosphoric acid-activated coconut shell adsorbents demonstrated effective uptake of Cu^{2+} and Mn^{2+} from acid mine drainage [13].

Bentonite-based composites have been widely reported for Hg^{2+} removal because of their high cation exchange capacity and surface functionality [14]. Bentonite, with its layered aluminosilicate structure and high cation-exchange capacity, provides abundant negatively charged sites for Hg^{2+} binding but tends to swell and agglomerate in water. In contrast, coconut shell-derived carbon contributes a highly porous structure and large surface area, offering extensive adsorption sites and stable pore channels for mass transfer. Coconut shell-derived activated carbons have been widely applied for the adsorption of various heavy metals such as Pb^{2+}, Cu^{2+} and Cr (VI), demonstrating the potential of agricultural waste as sustainable, biomass-based adsorbents. Integrating coconut shell carbon and bentonite into a monolithic composite mitigates recovery issues, improves porosity and structural integrity, and supports fixed-bed applications. This synergy combines the ion-exchange capacity of bentonite with the large surface area and pore structure of carbon, yielding and efficient, easily handled adsorbent for mercury and other heavy metals.

Hybrid adsorbents combining clay minerals and carbon biomass benefit from the porosity and ion-exchange synergy [15], with properties affected by filler size and loading. Incorporating coconut shell into adsorbent matrices improves thermal, structural and mechanical strength, yet the integration of bentonite and coconut shell into a single monolithic system for Hg^{2+} removal has not been explored.

This study addresses that gap by synthesizing and characterizing bentonite-coconut shell monoliths, activated physically and with HNO_3 to enhance performance [16] and to overcome challenges like low surface area and moisture resistance. The work highlights the material's efficiency, scalability and economic advantage over conventional adsorbents, positioning it as a practical candidate for sustainable mercury remediation. Therefore, this study aims to synthesize and characterize bentonite-coconut shell monoliths activated physically and with HNO_3, evaluates their Hg^{2+} adsorption performance via kinetics and isotherms and assesses production cost, offering a scalable and economical solution for sustainable mercury remediation.

Materials and methods

Materials

Coconut shell carbon was sourced from Banda Aceh, natural bentonite from Sigli, Indonesia and molasses was used as a binder. Mercury nitrate ($Hg(NO_3)_2$) was used to prepare mercury stock solutions. Nitric acid (HNO_3) served as the activating agent, while hydrochloric acid (HCl) and sodium hydroxide (NaOH) were applied for pH adjustment during adsorption test. All solutions were prepared using deionized water.

Purification and characterization of natural bentonite

Natural bentonite was purified by drying at 105 °C, grinding and sieving to < 75 μm particle size. The powdered bentonite was dispersed in deionized water (2 wt.%) and stirred continuously for 24 h. After sedimentation, the finer colloidal fraction rich in montmorillonite were separated by decantation. To remove carbonate and iron oxide impurities, the

suspension was treated with 1 M HCl, followed by repeated washing with 1 M NaCl to homoionize the bentonite into its sodium form. The samples were then washed with deionized water until chloride-free, oven-dried at 70 °C and stored in airtight containers.

Preparation of monolith adsorbents

Coconut shell charcoal was washed, dried, ground and sieved, then mixed with bentonite and molasses (6:3:1) to form a 100 g, 100-mesh blend. The mixture was molded into a 7-hole cylindrical (2 cm × 2 cm), air-dried for two days, and activated physically (600 °C, 3 h) or chemically (soaking in 0.5 or 1 N HNO_3 at 1.68 g: 100 mL for 2 h, room temperature, followed by drying at 110 °C). After drying and curing, the monoliths were rinsed to neutral pH and dried. The 7-hole design increases surface exposure, shorten diffusion paths, reduce pressure drop and maintains mechanical strength, giving better mass transfer and scalability than a solid block.

Characterization

Characterization included Fourier Transform Infrared Spectroscopy (FTIR, Bruker Tensor 27) over the range of 400 - 4,000 cm^{-1} for functional groups, Scanning Electron Microscopy (SEM, Hitachi TM3000) for morphology and Brunaeur-Emmet-Teller (BET, Micromeritics ASAP 2020) for surface area and pore size. These tests provided insight into the effects of chemical treatment on molecular structure and surface characteristics.

Adsorption investigation

Solution pH was measured with a calibrated pH meter immediately before and after adsorption; in all cases, the variation during contact time was less than $\pm$ 0.1 pH units. Batch adsorption studies were performed with 1.68 g of monolith in 250 mL of Hg^{2+} solution (2–8 mg/L) at pH 5, agitated at 100 rpm and 25 $\pm$ 1 °C for contact times of 30, 60, 90 and 120 min. The pH was adjusted using 0.1 M HCl or 0.1 M NaOH prior to contact with the adsorbent. Mercury concentrations were determined by atomic absorption spectroscopy (AAS, Analyst 800, Perkin Elmer, Co. USA) and removal and capacity were calculated using Eqs. (1) - (2). The effect of contact time, initial concentration and adsorbent type on mercury removal efficiency was studied. All investigations were performed in triplicate.

$$Adsorption\ (\%) = \frac{C_0 - C_t}{C_0} \times 100 \quad (1)$$

where: C_0 = Initial concentration of Hg^{2+} (mg/L)
C_t = Final concentration of Hg^{2+} after adsorption (mg/L)

$$q = \frac{(C_0 - C_t) \times V}{m} \quad (2)$$

where: q = Adsorption capacity (mg/g)
V = Volume of solution (L)
m = Mass of adsorbent used (g)

Isotherm models

The isotherm study tested Hg^{2+} concentrations of 2 - 8 mg/L to represent typical levels in rural groundwater and artisanal gold mining areas while avoiding precipitation issues at higher loadings. These conditions simulate realistic domestic and environmental applications in Aceh, Indonesia. Investigations used 1.68 mg of monolith in 250 mL Hg^{2+} solution, agitated at 110 rpm under controlled pH. Adsorption behavior was modeled using Freundlich, Langmuir and other isotherms by relating equilibrium concentration (C_e) to adsorbed mercury (q_e). The Freundlich model, suitable for heterogeneous surfaces and multilayer adsorption, expresses uptake as an exponential function of concentration without assuming a maximum capacit

The Freundlich model expresses adsorption on heterogeneous surfaces using Eq. (3) [17]:

$$q_e = K_F C_e^{\frac{1}{n}} \quad (3)$$

where q_e is the adsorbed amount, C_e the equilibrium concentration (mg/L), K_F the Freundlich capacity constant (mg/g) $(mg/L)^{-1/n}$ and 1/n the adsorption intensity (0 - 1 indicating favorable uptake). It is well suited for natural or activated carbon systems where multilayer adsorption can occur.

The Langmuir isotherm describes monolayer adsorption on uniform surfaces, assuming identical sites, constant adsorption energy and no interaction between adsorbed molecules, with equilibrium reached

when adsorption and desorption rates balance. Though first developed for gases, it is widely applied to liquid-phase systems to compare adsorption capacities and is useful for evaluating how well an adsorbent binds solute at defined, homogeneous sites.

The Langmuir model quantifies monolayer adsorption with Eq. (4) [18]:

$$q_e = \frac{q_m K_L C_e}{1 + K_L C_e} \quad (4)$$

where q_m is the maximum capacity (mg/g) and K_L the binding affinity constant (L/mg). Adsorption favorability is assessed by the dimensionless separation factor (R_L), given by Eq. (5):

$$R_L = \frac{1}{1 + K_L C_0} \quad (5)$$

with $0 < R_L < 1$ indicating favorable uptake.

Four additional isotherm models (Temkin, BET, Redlich-Peterson and Sips) were applied for comparison. Temkin assumes adsorption heat decreases linearly with coverage, expressed as Eq. (6):

$$q_e = \frac{RT}{b_T} \ln C_e + \frac{RT}{b_T} \ln K_T \quad (6)$$

where K_T is the binding constant (L/g) and b_T relates to sorption heat (kJ/mol).

BET extends Langmuir to multilayer adsorption, relating equilibrium concentration to monolayer capacity (q_m) and the BET constant (C_{BET}) linked to adsorption energy, as in Eq. (7):

$$\frac{C_e}{q_e(C_s - C_e)} = \frac{1}{q_m C_{BET}} + \frac{C_{BET} - 1}{q_m C_{BET}} \cdot \frac{C_e}{C_s} \quad (7)$$

where q_m is monolayer capacity (mg/g), C_{BET} = BET constant related to adsorption energy (dimensionless) and C_s = saturation concentration – for liquids this is set to solubility (mg/L).

The Redlich-Peterson and Sips models were applied to further assess adsorption behavior as in Eqs. (8) - (9):

$$q_e = \frac{K_R C_e}{1 + \propto_R C_e^{\beta}} \quad (8)$$

where K_R is capacity (L/g), α_R is affinity (L/mg) and β (0–1) bridge Langmuir ($\beta = 1$) and Henry's Law ($\beta = 0$).

$$q_e = \frac{q_m (K_s C_e^n)}{1 + K_s C_e^n} \quad (9)$$

where: q_m is maximum adsorption capacity (mg/g)
K_s is Sips equilibrium constant (L/mg)
n is heterogeneity factor, when $n = 1$, the model reduces to Langmuir.

To evaluate the goodness-of-fit of adsorption models, multiple statistical parameters were employed. A single error function, specifically the sum of squared errors (SSE), was used to evaluate the accuracy of the model fit [19] as appears in Eq. (10):

$$SSE = \sum_{i=1}^{n} \left(q_{e,calc} - q_{e,meas}\right)_i^2 \quad (10)$$

In addition to the sum pf squared errors (SSE), the coefficient of determination (R^2), root mean squared error (RMSE), and chi-square (χ^2) tests were calculated using the following equations:

$$R^2 = 1 - \frac{\sum (q_e - q_{e\,model})^2}{\sum (q_e - \overline{q_{e\,model}})^2} \quad (11)$$

$$RMSE = \sqrt{\frac{\sum (q_e - q_{e\,model})^2}{N}} \quad (12)$$

$$\chi^2 = \sum \frac{(q_e - q_{e\,model})^2}{q_{e\,model}} \quad (13)$$

where q_e and q_{model} represent experimental and calculated adsorption capacities, respectively, and N is the number of data points. This multi-criteria approach

provides a more reliable validation of model fitting than relying on a single statistical parameter.

Kinetic models

Kinetics were analyzed by the pseudo-first- and pseudo-second-order models. These models were selected because they are widely used, provide simple fitting procedures, and allow distinguishing between physisorption and chemisorption by comparing investigated and calculated adsorption capacities. The nonlinear formulations of these models are presented in Eqs. (14)-(15) [20,21]:

$$q_t = q_e(1 - e^{-k_1 t}) \quad (14)$$

$$q_t = \frac{q_e^2 k_2 t}{q_e k_2 t + 1} \quad (15)$$

In these models, q_e denotes the amount of adsorbate adsorbed at equilibrium.

Results and discussion

Characterization of adsorbents

XRD analysis confirms montmorillonite as the dominant phase in bentonite (**Figure 1**), indicated by the strong basal reflection at 2θ ≈ 6 - 7°, corresponding to a d-spacing of ~12 - 14 Å, characteristic of smectite minerals. Additional reflections at 2θ ≈ 20.3° and 26.6° (d = 3.34 Å) are assigned to quartz impurities, while weaker peaks around 28 - 29° and 36° suggest the presence of aluminosilicate structures, likely feldspar. Minor high-angle peaks (> 60°) further support the occurrence of quartz and no detectable mercury contamination. The absence of calcite, kaolinite, or metallic oxides indicates their negligible presence in the sample.

FTIR spectra identified characteristic Si-O-Si stretching (1,045 cm^{-1}), Al-OH/Mg-OH bands (3,641 cm^{-1}) and Si-O-Si and Si-O-Al bending confirming the presence of montmorillonite, while the absence of carbonate peaks (~1,430 cm^{-1}) indicated successful purification (**Figure 1**). These results collectively confirmed that purification process successfully enhanced the quality of the natural bentonite by enriching its montmorillonite content, reducing impurities and improving surface characteristics, making it suitable for mercury adsorption studies

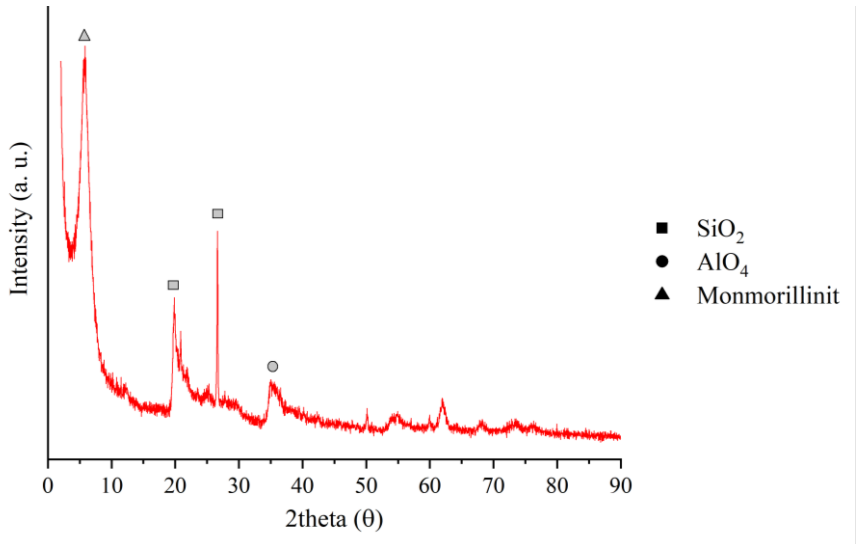

Figure 1 XRD pattern represents the crystalline phases present in the bentonite sample.

FTIR analysis for monolith showed the presence of functional groups corresponding to hydroxyl (-OH), carbonyl (C=O) and siloxane (Si-O-Si) stretching bands, which enhance the adsorption of Hg^{2+} ions, with shifts indicating successful chemical activation. All adsorbents exhibited spectral features similar to typical bentonite, although notable shifts in several absorption peaks were observed. For instance, the Si-O stretching

vibration typically available at 1,042 cm^{-1} in bentonite appeared at 1,016 cm^{-1}, 1,030 cm^{-1} and 1,024 cm^{-1} for monolith activated physically, with 0.5 N HNO_3, and 1 N HNO_3, respectively. Acid treatment shifted Si-O stretching peaks and introduced nitrate groups, confirming surface modification and enhanced oxygen-containing functionalities favorable for Hg^{2+} binding.

Table 1 presents the wavenumber ranges of characteristic bonds associated with certain functional groups. The FTIR spectra of the monoliths treated with various concentrations of nitric acid (0.5 N and 1 N) show distinct changes in transmittance across key wavenumber regions. Further analysis of the FTIR spectra at specific wavenumbers reveals the following: The peak around 474 cm^{-1} corresponds to silicate [22] bending vibrations (such as Si-O-Al or Si-O-Mg), indicating the structural presence of bentonite.

The band near 1,024 cm^{-1} is attributed to Si-O-Si stretching, characteristic of silicate structures, and shifts in this region reflect changes because of acid treatment. The alteration in the IR spectra following Hg^{2+} adsorption confirm effective interaction between the monolith and Hg^{2+} ions, as evidenced by noticeable shift and decreased peak intensities. Similar patterns have been reported in earlier research [23].

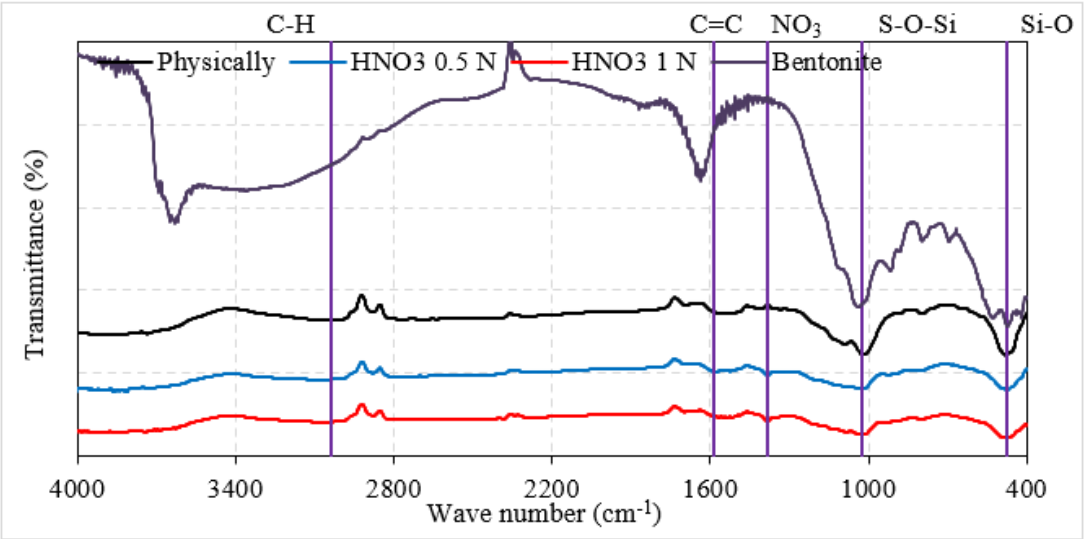

Figure 2 FTIR spectra of bentonite and monolith adsorbent treated physically and with HNO_3.

Additionally, a broad peak around 3,435 cm^{-1} in bentonite is associated with the O-H groups from Al-OH in the material structure. However, these particular bands were either diminished or absent in the monolith adsorbents, likely because of interactions between coconut shell components. The disappearance of the external O-H band, which is prominent in raw bentonite but missing in the composites, is attributed to heat treatment during preparation. The 1,385 cm^{-1} peak represents symmetric stretching of nitrate (NO_3^-) groups, confirming their incorporation following HNO_3 activation. At 1,584 cm^{-1}, absorption is linked to C=C aromatic ring or asymmetric COO^- stretching, which intensifies in acid-treated samples, indicating enhanced carboxyl or aromatic character. Lastly, the 3,040 cm^{-1} band is assigned to C-H stretching of aromatic rings, suggesting the preservation and light modification of the coconut shell-derived carbon matrix.

Table 1 FTIR wavenumber range of monolith adsorbent.

Wavenumber (cm^{-1})	Band Assignment	Interpretation
3,040	C-H stretch (aromatic rings)	More visible in red (1 N) and blue (0.5 N), indicating the preservation and light modification of the coconut shell-derived carbon matrix
1,584	C=C or COO^- stretching	Stronger in acid-treated samples, suggests enhanced carboxyl or aromatic character

Wavenumber (cm^{-1})	Band Assignment	Interpretation
1,385	NO_3	NO_3^- incorporation
1,024	Si-O-Si stretch (silicate structure)	Peak sharpening in acid-treated samples, indicates structural modification, likely because of acid treatment
474	Si-O bending vibrations	More defined after HNO_3 treatment, points to the structural presence of bentonite

Figure 3 displays SEM images of bentonite and monolith activated physically and with 1 N HNO_3 at 7000×, 5000×, 350× and 800× magnification, respectively. SEM images revealed the transformation from layered bentonite (**Figure 3(a)**) into monoliths with irregular, heterogeneous pores after physical activation and a more fragmented, porous morphology (**Figure 3(b)**) following HNO_3 treatment, which increased surface roughness and exposure of adsorption sites. The surface in **Figure 3(a)** consists of irregular platelets and aggregated clusters, forming micro-porous channels and interparticle voids. These structural features enhance surface accessibility and provide potential pathways for adsorbate diffusion.

The rough and heterogeneous texture in **Figure 3(b)** also suggests the presence of active functional groups, contributing to cation exchange and chemical interaction processes. Particle morphology also varied, with non-uniform sizes and shapes.

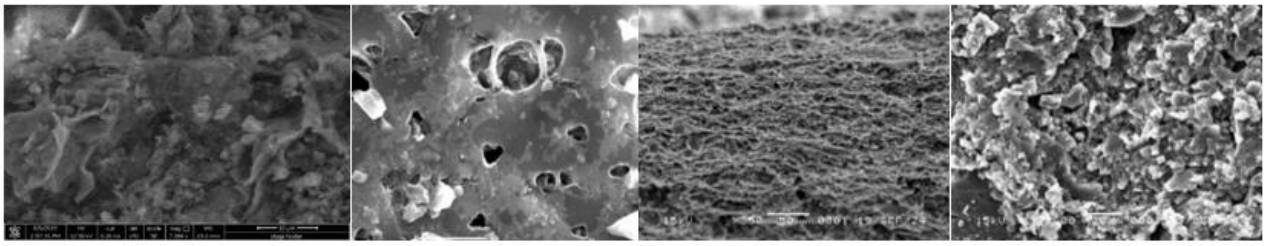

(a) (d) (c) (d)

Figure 3 SEM micrograph of (a) bentonite, monolith activated (b) physically, with 1 N HNO_3 at (c) 350× and (d) 850×.

SEM images showed irregular pores with greater development in chemically activated samples. SEM micrographs revealed increased porosity in the acid-activated monoliths. After chemical activation with HNO_3, the morphology of monolith undergoes a noticeable transformation (**Figure 3(c)**). This change can be attributed to partial dissolution of impurities and modification of the aluminosilicate framework, which increases pore volume and exposes additional adsorption sites. It explains the improved adsorption performance observed in the study. These observations align with previous reports where acid treatment significantly modified the surface texture of bentonite, improving its adsorption efficiency by increasing both surface area and the accessibility of functional groups.

BET analysis showed increased surface area in chemically activated monoliths, supporting improved adsorption performance. BET results showed a modest surface area increase from 20.97 mg/g (physically activated) to 23.78 m^2/g (1 N HNO_3-treated), accompanied by reduced pore radius (1.8142 nm) compared to the physically treated monoliths (2.0457 nm) because of micropore development. It confirms enhanced porosity that contributed to higher adsorption. Although the surface area (20 - 23 m^2/g) is lower than natural bentonite (**Table 2**), the monolithic geometry, synergistic bentonite-carbon structure and functional group enrichment improve mass transfer and adsorption potential. Moreover, the low production cost and high mechanical strength ensure practical applicability, thereby offsetting the limitations of modest surface area.

Table 2 Characteristics of bentonite and monoliths treated physically and 1 N HNO_3 activation.

Component	Surface area (m^2 g^{-1})	Pore size (nm)	Pore volume (cm^3 g^{-1})
Bentonite	93.150	6.4500	2.4020
Monolith activated physically	20.966	2.0457	0.1094
Monolith activated with 1 N HNO_3	23.780	1.8142	0.1608

Despite this, the pore sizes of the monoliths were reduced compared to pure bentonite, attributed to biomass incorporation and structural compaction. Nonetheless, their surface characteristics still suggest good potential for Hg^{2+} removal. The reduction in pore size compared to raw bentonite is attributed to the monolithic structure and incorporation of coconut shell biomass. It classified the adsorbents as mesoporous materials with enhanced surface area following chemical treatment. Acid activation enhanced carboxyl and nitrate features, narrowed pores, and increased microporosity, collectively supporting stronger Hg^{2+} uptake despite modest surface area. This shift from mesoporous structures toward micropores character improves the accessibility of adsorption sites for mercury ions and results in a better surface-to-volume ratio, which is beneficial for adsorptive interactions.

Adsorption performance

The study evaluated mercury adsorption by bentonite-coconut shell monoliths at a controlled temperature of 25 °C to avoid thermal effects. Adsorption efficiency rose with contact time and initial Hg^{2+} concentration, peaking around 120 min, especially for acid-activated monoliths. **Figure 4** illustrates that the selected Hg^{2+} concentrations (2 and 6 mg/L) corresponds to typical levels found in groundwater affected by artisanal and small-scale hold mining in rural Southeast Asia. Acid activation with HNO_3 significantly improved performance: The 1 N HNO_3 monolith removed 90.19% of Hg^{2+} (reducing 2 mg/L to 0.21 mg/L, capacity of 0.286 mg/g), while 0.5 N HNO_3 achieved 70.09% at 2 mg/L and 78.71% at 6 mg/L. Physically activated samples removed only ~38%.

After treatment with the chemically activated monolith (0.5 N HNO_3), the final concentration of 6 mg/L mercury solution decreased significantly to approximately 1.32 mg/L. In comparison, the physical activated monolith reduced the mercury concentration to 3.89 mg/L. This trend is attributed to the high availability of active adsorption sites at the beginning, which gradually became occupied, resulting in a slower increase in overall adsorption efficiency [24].

Chemical etching introduced oxygen-containing groups and enhanced microporosity, thereby improving adsorption performance. Enhanced removal is linked to surface oxidation, and introduction of – COOH and -OH groups, increased microporosity and higher surface area from HNO_3 treatment, despite smaller pore radii. This trend confirms the effectiveness of nitric acid activation in promoting fast and efficient mercury adsorption. Looking ahead, it is important to place these findings in the broader context of real-world wastewater scenarios.

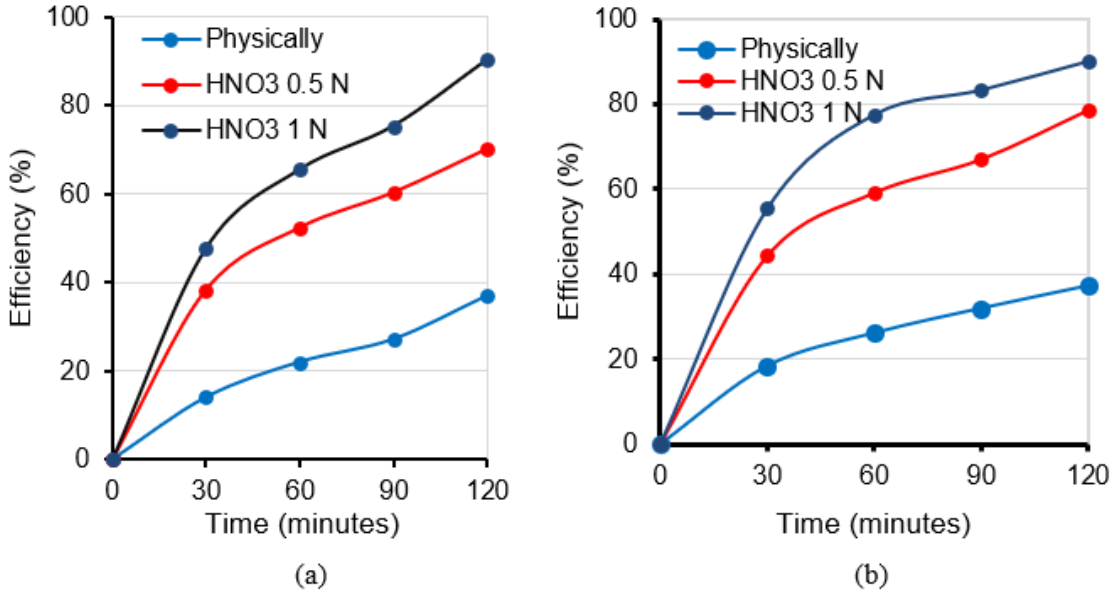

Figure 4 The effect of time on the adsorption for Hg^{2+} concentrations of (a) 2 and 6 mg/L.

Targeting 2 - 6 mg L^{-1} mirrors typical artisanal mining effluents, supports rural relevance, and is relevant to local discharge standards, but future work will assess higher mercury levels (e.g. 10 - 50 mg L^{-1}) to address industrial wastewater scenario.

Adsorption isotherms

The isotherm study evaluated Hg^{2+} uptake on bentonite-coconut shell monoliths using six models (Langmuir, Freundlich, Temkin, BET, Redlich-Peterson, Sips). The fitting parameters and sum of squared error (SSE) values are summarized in **Table 3**. Freundlich model assumes that the adsorbent's active sites vary in energy. Isotherm studies indicated that Freundlich model (SSE = 0.00004) accurately described adsorption on physically activated bentonite-coconut shell monolith, suggesting multilayer uptake on a heterogeneous surface, while the Langmuir model better fit the data after chemical activation, reflecting monolayer adsorption on more uniform sites. This suggests the coexistence of multilayer and monolayer adsorption.

Table 3 Parameters of adsorption isotherm models for Hg^{2+} onto activated monoliths

Isotherm model	Parameters	Activated Physically	1 N HNO_3
Freundlich	K_F (mg/g) $(mg/L)^{-1/n}$	0.086	1.260
	n	0.963	1.111
	SSE	**0.00004**	0.004
	R^2	**0.999**	0.988
	RMSE	**0.002**	0.001
	χ^2	**0.00009**	0.004
Langmuir	q_m (mg/g)	6.035	7.235
	K_L (L/mg)	0.085	1.448
	SSE	0.005	**0.002**
	R^2	0.921	**0.993**
	RMSE	0.035	**0.025**
	χ^2	0.014	**0.003**

Isotherm model	Parameters	Activated Physically	1 N HNO_3
Temkin	b_T (kJ/mol)	9.911	4.629
	K_T (L/mg)	1.098	7.610
	SSE	**0.002**	0.005
	R^2	0.962	**0.985**
	RMSE	0.024	**0.035**
	χ^2	0.010	**0.010**
BET	C_{BET} (L/mg)	1.332	11.435
	q_s (mg/g)	3.203	6.337
	SSE	**0.00002**	0.002
	R^2	**1.000**	0.993
	RMSE	**0.002**	0.025
	χ^2	**0.00004**	0.003
Redlich-Peterson	K_R (L/g)	0.093	1.280
	α_R (L/mg)	0.010	0.008
	β	0.001	0.001
	SSE	**0.004**	0.020
	R^2	**0.949**	0.991
	RMSE	**0.031**	0.071
	χ^2	**0.014**	0.032
Sips	q_m (mg/g)	11.725	0.880
	K_s (L/mg)	0.021	0.400
	n	1.381	0.700
	SSE	**0.001**	1.058
	R^2	**0.987**	0.519
	RMSE	**0.016**	0.514
	χ^2	**0.007**	4.278

The Temkin isotherm demonstrated a moderate fit to investigated data, with the Temkin constant b_T of 10.144 kJ/mol. Temkin suggests that the heat of adsorption decreases linearly with coverage, indicating that both physisorption and chemisorption contribute. The relatively high value of 1.098 L/mg further supports the homogeneous active sites on the adsorbent surface.

The BET model describes multilayer adsorption, provided a strongest correlation with the experimental data (SSE = 0.00002). This is expected since Hg^{2+} adsorption in aqueous solutions is predominantly multilayer-driven and multilayer adsorption is not limited because of the ionic nature and solubility of mercury in water.

Redlich-Peterson and Sips show poor fit for these systems. The Redlich-Peterson model yielded an exponent (β) of 0.001, which is far from unity, indicating that the system does not follow a Langmuir-type adsorption at the tested concentration range. The error value (SSE = 0.004) further confirmed the unsuitability of this model.

The Sips isotherm provided the better overall description of the investigated data, with the lower SSE (0.001). The heterogeneity factor n was calculated as 1.381, which is more that unity, signifying that adsorption occurred on energetically homogeneous sites. After physical activation, the adsorption behavior resembled Freundlich-type multilayer adsorption, whereas chemical activation shifted it toward Langmuir-

type monolayer adsorption, confirming the hybrid nature of the process.

While previous evaluations relied solely on SSE, incorporation of R^2, RMSE and χ^2 provides stronger evidence of model reliability. Physically activated monoliths fit the Freundlich (R^2 = 0.999, SSE = 0.00004, RMSE = 0.002, χ^2 = 0.00009) and BET (R^2 = 1.000, RMSE = 0.002, χ^2 = 0.00004) models best, indicating multilayer adsorption on heterogeneous sites with limited surface functionalization and lower capacity (6.035 mg/g). Chemically activated monoliths (1 N HNO_3) fit the Langmuir model (R^2 = 0.993, q_m = 7.235 mg/g, RMSE = 0.025, χ^2 = 0.003), reflecting monolayer adsorption on a more uniform sites created by acid treatment. Freundlich approximates the trend but deviates at high q_e (**Figure 5**). Models such as Sips exhibited poor fit (R^2 = 0.519), confirming their inadequacy in describing the system.

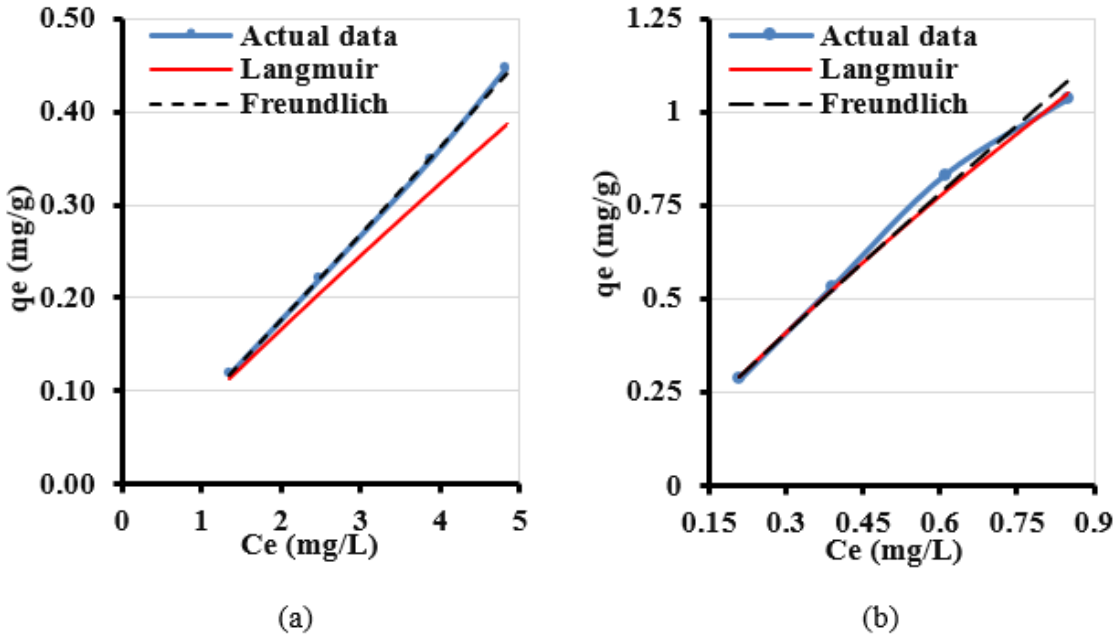

Figure 5 Isotherm on the adsorbent with: (a) physical activation and (b) 1 N HNO_3 activation.

These results highlight that combining multiple statistical indicators allows more robust discrimination of adsorption mechanism compared to using SSE alone. **Figure 5(a)** shows the adsorption isotherm for the monolith with physical activation. The adsorption data are fitted using Langmuir (red line) and Freundlich (black dashed line) models. This indicates multilayer adsorption behavior on a heterogeneous surface, which is typical of unmodified or untreated adsorbents. Adsorption data for physically activated monoliths fit the Freundlich model, indicating multilayer adsorption on heterogeneous surfaces. This suggest that the physical treated monolith has diverse active sites with varying affinities, which is typical of materials that have not undergone chemical modification. The relatively low adsorption capacity further reflects the limited number of available active sites. The adsorption of Hg^{2+} on inactivated monolith is non-ideal and multilayer, with varying surface energies. The Langmuir model exhibited clear deviation from the actual adsorption data, especially for chemically activated bentonite-coconut shell monolith, indicating that ideal monolayer assumptions are only partially met.

Figure 5(b) presents the isotherm for the monolith activated with 1 N HNO_3. Chemically activated samples followed the Langmuir isotherm, suggesting monolayer adsorption. The Langmuir curve closely follows the actual data points across the full range of equilibrium concentrations (C_e). This indicates that the adsorption process is better described by Langmuir assumptions, suggesting a monolayer adsorption on a homogeneous surface with single sites. This result is consistent with the improved adsorption performance observed in the kinetic studies and supports the interpretation that

chemical activation enhances the availability and uniformity of active sites on the adsorbent, leading to behavior consistent with Langmuir characteristics. This demonstrated the effectiveness of nitric acid activation in improving adsorption performance.

All Langmuir separation factor (R_L) values lie between 0 - 1, confirming favorable adsorption [25]. It is an important indicator in the Langmuir isotherm, calculated using the initial concentration (C_0) and the Langmuir constant (K_L) as shown in Eq. (5). This factor indicates how favorable the adsorption process is. Adsorption is unfavorable when $R_L > 1$, irreversible when $R_L = 0$ and linear if R_L is around 1. R_L varies with C_0, where all values fall within the 0 - 1 range, confirming that the adsorption of Hg^{2+} onto the monolith is still favorable.

In summary, the best-fitting model of adsorption with physical activation is Freundlich with multilayer adsorption type, minimal surface functionalization, varying adsorption site uniformity, but homogeneous surface condition. These findings also confirm that chemical activation using nitric acid enhances the adsorption efficiency and structural regularity of the adsorbent, which is beneficial for mercury removal from aqueous solutions.

The Langmuir model produced a seemingly high maximum capacity (7.23 mg/g) for chemically activated samples. The Langmuir model was a better fit only for chemically activated monoliths, which exhibited more uniform surface sites because of nitric acid treatment. It can be clarified that the Freundlich model provides a more accurate reflection of adsorption behavior for natural, unmodified materials.

Overall, the results highlight that while the Langmuir and Freundlich models provide a preliminary understanding of the system, the BET and Sips models offer a more comprehensive description of Hg^{2+} adsorption on bentonite-coconut shell monoliths. This confirm that the adsorption process is controlled by homogeneous surface interactions, with strong affinity at low concentrations and finite site saturation at higher concentrations.

The variations in adsorption capacity are likely because of differences in the adsorbents' characteristics, including surface area, porosity, and pore size. Additionally, the match between the adsorbent's pore size and the molecular size of Hg^{2+} can significantly influence the adsorption performance for different pollutants. As summarized in **Table 3**, the monolith's uptake (7.235 mg/g) lies the lower range of reported Hg^{2+} capacities but remains comparable to several low-cost mineral, underscoring the scope for future functionalization and porosity tuning. For example, sulfuric magnetic biochar reaches 8.93 mg g^{-1} [26], whereas bentonite-based monoliths tested as structured bodies can show ~0.2 mg g^{-1} performance [27], reflecting diffusion/geometry limits and lower functional-group density. The advantages of this adsorbent lie in simple synthesis. Future improvements should target reducing intraparticle resistance to bridge the gap with S-rich carbons/silicas.

The adsorption mechanism of Hg^{2+} ions onto bentonite-coconut shell monolith are summarized in **Figure 6**. The layered bentonite structure, dominated by Si-O and Al-O frameworks, provides negatively charged surfaces. This confirms that the adsorption process is controlled by homogeneous surface interactions, with strong affinity at low concentrations and finite site saturation at higher concentrations. These interactions are consistent with the pseudo-first-order kinetic model obtained in this study, which suggest that adsorption primarily occurs through homogeneous surface sites with similar binding mechanisms.

Nitric acid activation introduces -COOH and -OH groups, increases surface homogeneity and metal binding affinity, and shifts behavior from multilayer adsorption on heterogeneous sites to monolayer on more uniform surfaces. Despite moderate capacity compared with sulfur-rich carbons, the monolith's low cost, easy separation, and low pressure drop make it practical. Mechanistically, Hg^{2+} binds via cation exchange within bentonite layers, surface complexation on Si-OH/Al-OH groups, hydrogen bonding, π-π interactions, and diffusion through the coconut-shell carbon matrix. Thus, the synergy between bentonite's mineral-based adsorption and coconut shell's carbonaceous functionalities accounts for the high removal efficiency and adsorption capacity reported in this work.

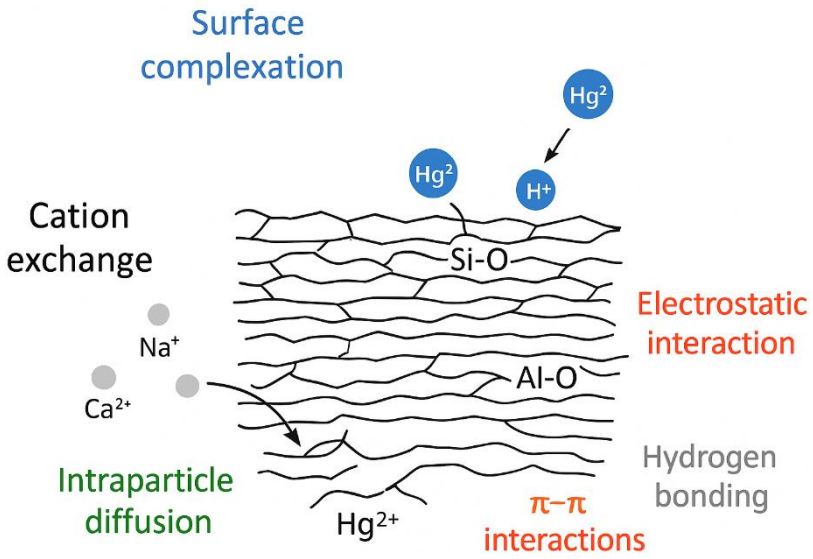

Figure 6 Illustrative diagram showing the possible adsorption mechanism.

Adsorption kinetics

The kinetics study assessed Hg^{2+} uptake on bentonite-coconut shell monoliths (physically activated, 0.5 N HNO_3, 1 N HNO_3) using pseudo-first-order and pseudo-second-order models. The kinetics of adsorption were analyzed to understand both the rate and underlying mechanism of the process. **Table 4** presents the kinetic parameters derived from fitting various models to the experimental data for Hg^{2+} adsorption onto the three adsorbents. Adsorption was rapid, reaching near-equilibrium within ~90 - 120 min, indicating strong interactions between Hg^{2+} and adsorbents. To determine which model best represented the experimental data, sum of square error was used as the selection criterion – where a lower SSE value suggests a better model fit. Pseudo-first-order provided the best fit (e.g. SSE = 0.0004, R^2 = 0.999 and q_e model = 0.0975 mg/g, and q_e exp = 0.118 mg/g), with modeled q_e values close to experiment, indicating that physisorption on homogeneous sites dominates (**Table 4**).

Table 4 Kinetic model for the Hg^{2+} adsorption onto adsorbents with physical and HNO_3 activation.

Kinetic model	Parameters	With physical activation		Activated with 0.5 N HNO_3		Activated with 1 N HNO_3	
		2 mg/L	6 mg/L	2 mg/L	6 mg/L	2 mg/L	6 mg/L
Pseudo-first order	q_e exp (mg/g)	0.118	0.348	0.223	0.726	0.286	0.832
	q_e model (mg/g)	0.098	0.321	0.2066	0.6675	0.2590	0.8070
	k_1 (min^{-1})	0.015	0.021	0.022	0.021	0.020	0.029
	SSE	**0.0004**	**0.0008**	**0.0005**	**0.0091**	**0.0013**	0.0021
	R^2	**0.999**	**0.996**	**0.995**	**0.996**	**0.996**	0.990
Pseudo-second-order	q_e exp (mg/g)	0.118	0.348	0.223	0.726	0.286	0.832
	q_e model (mg/g)	0.095	0.295	0.193	0.631	0.2476	0.751
	k_2 (min·g/mg)	**0.303**	**0.133**	**0.241**	**0.076**	**0.191**	**0.093**
	SSE	0.0008	0.0042	0.0012	0.0113	0.0022	**0.0141**
	R^2	0.975	0.988	0.988	0.984	0.977	**0.997**

Pseudo-second-order fit some data at 6 mg/L but generally showed higher SSE (0.0008) and poorer curve matching (q_e model = 0.095 vs. q_e exp = 0.118 mg/g), suggesting limited chemisorption contribution. The superior fit of the pseudo-first-order demonstrates that physisorption is the dominant rate-controlling step. The relatively low k_2 values supported this conclusion. Differences in adsorption rates were consistent with changes in surface area and porosity.

Figures 7(a) and **7(b)** illustrate the adsorption kinetics of mercury (Hg^{2+}) ions at an initial concentration of 2 mg/L, comparing different monolith adsorbents: Without activation (red triangles), activated with 0.5 N HNO_3 (blue circles), and activated with 1 N HNO_3 (black squares). Each graph is fitted using a different kinetic model.

Pseudo-first-order model assumes the rate of adsorption is directly proportional to the number of unoccupied adsorption sites. The curve for 1 N HNO_3 fits well with the model, suggesting fast occupation of available active sites. Chemically activated monoliths reached equilibrium more rapidly and removed more Hg^{2+} than the physically activated samples. Pseudo-second-order model is based on the assumption that adsorption is controlled by chemisorption, involving valence forces or electron sharing between adsorbent and adsorbate. The 1 N HNO_3-activated monolith had the highest capacity (q_t = 0.286 mg/g) and fastest uptake, followed by 0.5 N HNO_3; physically activated samples showed lowest rates and capacities, indicating limited surface area and fewer active sites. The data points closely match the fitted curves, particularly for physically activated samples. The better fit of the first-order model (especially for physically activated adsorbents) indicates that physisorption is likely the dominant mechanism.

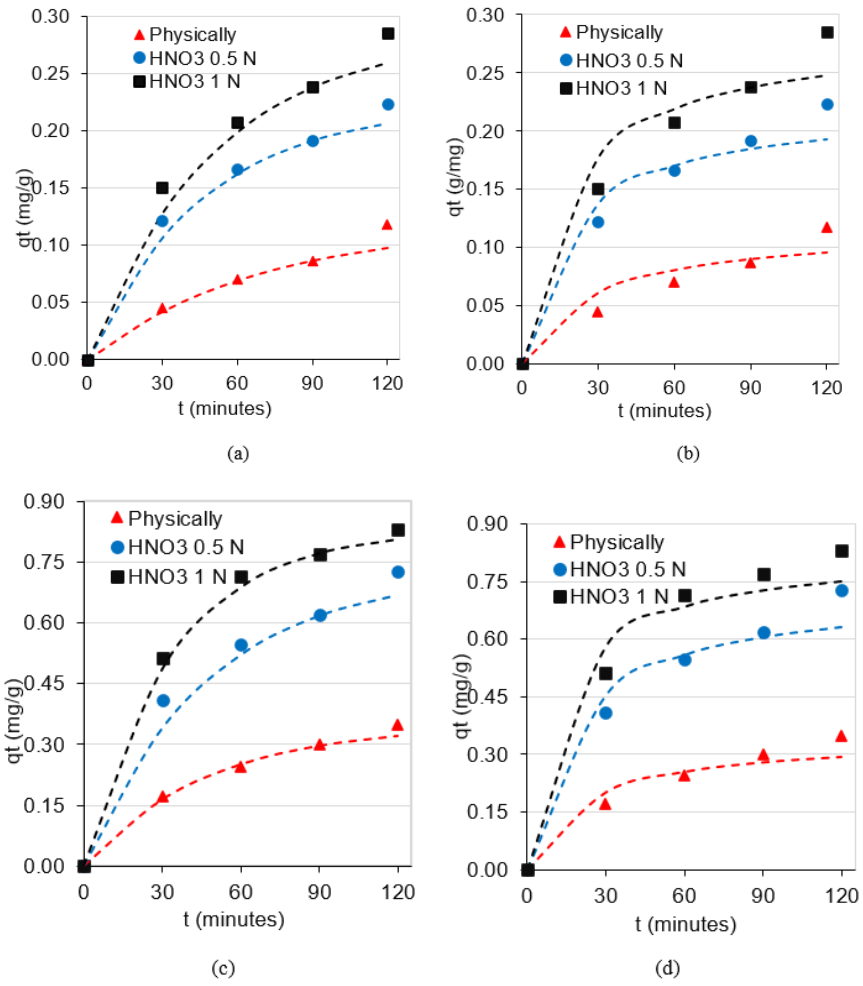

Figure 7 Adsorption kinetics at a concentration of 2 mg/L for (a) pseudo-first-order, (b) pseudo-second-order and at 6 mg/L for (c) pseudo-first-order, and (d) pseudo-second-order.

Acid activation improved kinetics through increased surface area, pore structure and -OH/-COOH functional groups. Among the two models, the pseudo-first-order gives a better overall fit, especially for physically activated adsorbents, indicating physisorption as the primary mechanism.

Figures 7(c) and **7(d)** illustrate the adsorption kinetics of Hg^{2+} at an initial concentration of 6 mg/L onto adsorbents with different activation conditions (without activation, with 0.5 N HNO_3 and 1 N HNO_3), modeled using pseudo-first-order kinetics and pseudo-second-order kinetics. In **Figure 5(c)**, q_t (mg/g) increases with time for all adsorbents, indicating progressive mercury adsorption. Black squares (HNO_3 1 N) show the highest adsorption capacity, reaching 0.286 mg/g at 120 min. Blue circles (HNO_3 0.5 N) follow, achieving 0.223 mg/g. Red triangles (with physical activation) exhibit the lowest performance, only 0.118 mg/g. The curve fitting suggests that the pseudo-first-order model fits the experimental data, especially at higher times, particularly for the HNO_3 1 N sample, indicating a deviation from first-order kinetics. This model assumes that the adsorption rate is proportional to the number of unoccupied sites. The low fit implies that this assumption may not capture the actual adsorption mechanism, especially for activated adsorbents with heterogeneous surface sites.

In **Figure 7(d)**, q_t (mg/g) vs. t (min) still increases in the same trend for all adsorbents. The pseudo-second-order model gives a much worse fit to the experimental data across all activation levels. The curves do not match the data points closely, particularly for the HNO_3 1 N and 0.5 samples. This suggests that chemisorption is not the dominant rate-limiting step, involving valence forces or electron sharing between Hg^{2+} and the adsorbent surface.

The pseudo-first-order model better describes the adsorption behavior of Hg^{2+} at 6 mg/g, indicating that the mechanism likely involves physisorption rather than simple chemical uptake. The chemically activated bentonite-coconut shell monoliths showed faster equilibrium and higher removal capacity.

The study did not yet test regeneration or mechanical stability. Literature indicates similar bio-adsorbents retain 70 - 85% capacity for 3 - 5 cycles with 0.1 M HCl or NaCl desorption. Regeneration and reuse studies are underway and will be reported in a separate publication, as the present work primarily aimed to establish baseline adsorption performance and isotherm/kinetic characteristics.

Although monoliths are well-suited for continuous flow treatment, this study did not evaluate their mechanical performance under wet and pressurized conditions. These factors are crucial for continuous-flow systems. Given their intended use in continuous-flow systems, future work should involve compressive strength testing (e.g., ASTM C1424) and slake durability tests (e.g., ASTM D4644) to ensure stability during continuous flow operation. Because this work focused on establishing baseline adsorption performance, mechanical stability under wet and flow conditions has not yet been assessed; this evaluation is ongoing and will be reported separately.

Cost estimates (US$0.76 - 1.36 kg^{-1}) confirm economic feasibility versus other monoliths and bulk activated carbo (~US$0.4 - 5 kg^{-1}). This composite material is naturally abundant, locally sourced, and requires minimal processing, which contributes to reduced operational and energy expenditure. To support the claim of low-cost applicability, a theoretical cost breakdown was developed. Estimated costs per kg of bentonite-coconut shell monolith are as follows: Bentonite ($0.02 - 0.05), coconut shell charcoal ($0.05 - 0.13), molasses binder ($0.03 - 0.06), fuel for drying ($0.03 - 0.06), labor ($0.06 - 1.00) and equipment ($0.02 - 0.05).

Commercial activated carbon prices vary strongly with grade, form, and order quantity. Bulk powder or granular activated carbon is commonly priced on the order of ≈US$1.5 - US$6.3 per kg (regional/grade variation), whereas small retail/laboratory packs are substantially more expensive on a per kg basis (tens to hundreds of US$ per kg). Therefore, for economic comparisons, this study used a conservative bulk price of ≈US$2 kg^{-1} (≈US$0.002 g^{-1}) unless otherwise stated. Prices were surveyed from commercial bulk listings and market reports [30]. The use of locally materials and low activation costs makes this method economically feasible for rural and industrial wastewater treatment applications. **Table 5** compares bentonite-coconut shell monolith with other monoliths. Current tests used single-component Hg^{2+} solutions. In real systems, other

ions may compete for active sites. The current single contaminants study limits conclusions about bentonite-coconut shell monolith selectivity. Future research will include competitive adsorption (Pb^{2+}, Cd^{2+}, Cl^-, NO_3^-) and higher-strength mechanical testing for continuous-flow applications.

Table 5 Benchmarking bentonite-coconut shell monolith vs. other monoliths.

Material	Cost (US$/kg)	BET Surface Area (m^2/g)	Maximum Adsorption Capacity (mg/g)	Mechanical Strength	Typical Kinetics/ Isotherm
Bentonite-coconut shell (1 N HNO_3)	0.76 - 1.36	~20 - 30	~7.23	Moderate (untested under flow)	Pseudo-first order; Freundlich
Clay-carbon-MnO_2 [28]	2 - 5	Not specified	~1.18 (Hg, Langmuir q_m)	Moderate (untested under flow)	Pseudo-first-order; Langmuir
Clinoptilolite Zeolite Monolith [29]	~2.5	~31	~27 (dye adsorption)	~14 MPa compressive strength	Langmuir (monolayer dye adsorption)

Conclusions

The study confirms that bentonite-coconut shell monoliths are effective, low-cost adsorbents for Hg^{2+} removal. Acid activation with 1 N HNO_3 enhanced surface area, functional groups, and adsorption capacity, achieving up to 7.235 mg/g. Kinetic analysis showed rapid initial uptake governed mainly by pseudo-first-order behavior, with slower intraparticle diffusion at later stages as the sites become saturated. Isotherm modeling indicated Freundlich behavior for physically activated samples and a Langmuir fit after chemical activation, reflecting a shift from multilayer to monolayer adsorption. Production costs (~$0.76 - 1.36/kg) are far below conventional activated carbon, supporting economic viability. Overall, the monoliths provide fast, efficient, and sustainable mercury removal, suitable for industrial wastewater treatment. Future work will address higher contaminant levels, regeneration and reuse, competing ions, mechanical testing and surface modification guide scale-up.

Acknowledgements

This research was funded by a Professor Research grant from Ministry of Education, Culture, Research and Technology of Indonesia and LPPM of Universitas Syiah Kuala (No. 72/UN11.2.1/PG.01.03/SPK.PTNBH/2024).

Declaration of generative AI in scientific writing

The authors acknowledge utilizing generative AI tools (e.g., OpenAI's ChatGPT) solely for language refinement and grammar correction during the preparation of this manuscript. The AI tool was not used for content creation or data interpretation. The authors assume full responsibility for all content and conclusions presented in this work.

CRediT author statement

Darmadi: Conceptualization; Methodology; Supervision; Validation. **Mirna Rahmah Lubis**: Data curation; Validation; Writing - Original draft preparation; Writing - Reviewing and Editing. **Adisalamun**: Data curation; Formal analysis; Investigation; Project administration; Software; Validation. **Muhammad Zaki**: Data curation; Funding acquisition; Formal analysis; Resources; Validation; Visualization.

References

[1] H Jeong, W Ali, P Zinck, S Souissi and JS Lee. Toxicity of methylmercury in aquatic organisms and interaction with environmental factors and coexisting pollutants: A review. *Science of The Total Environment* 2024; **943**, 173574

[2] GP Yoga, AA Sari, IS Nurhati, Yustiawati, Andreas and D Hindarti. Mercury contamination

on aquatic organisms in related to artisanal small-scale gold mining activity in Indonesia: A mini review. *IOP Conference Series: Earth and Environmental Science* 2022; **1062**, 012023.

[3] N Aflah, Mulkal, H Sentiya, F Yunining, IN Aslam, Muchlis and H Harisman. Mapping the spread of mercury from artisanal mining activities in Aceh Jaya through geochemical surveys. *Journal of Chemical Engineering & Environment* 2023; **18(1)**, 9-18.

[4] KG Pavithra, P Sundarrajan, PS Kumar and G Rangasamy. Mercury sources, contaminations, mercury cycle, detection and treatment techniques: A review. *Chemosphere* 2023; **312(P1)**, 137314.

[5] S Satyam and S Patra. Innovations and challenges in adsorption-based wastewater remediation: A comprehensive review. *Heliyon* 2024; **10(9)**, e29573.

[6] EPA. *Mercury: Human Exposure and Health Effects 2020*. U.S. Environmental Protection Agency.

[7] TE Oladimeji, M Oyedemi, ME Emetere, O Agboola, JB Adeoye and OA Odunlami. Review of the impact of heavy metals from industrial wastewater effluent and removal capacities. *Heliyon* 2024; **10(23)**, e40370.

[8] SE Pour, AH Mamaghani and Z Hashisho. Modeling of adsorption process on monolith adsorbent: A mini-review. *Separation and Purification Technology* 2025; **354(P2)**, 128846.

[9] MI Shaukat, NRB Rosli, R Wahi, SMAA Abdullah and Z Ngaini. Chemically modified coconut shell biochar for removal of heavy metals from aqueous solution. *Defect and Diffusion Forum* 2021; **411**, 79-91.

[10] S Zahra, Z Mahmood, F Deeba, A Sheikh, H Bukhari and H Mehtab. Modifications of coconut shell charcoal for metal removal from aqueous solutions. *European Journal of Chemistry* 2022; **13(3)**, 259-266.

[11] P Kumar and JK Srivastav. Comparative analysis of coconut shell and iron-impregnated activated carbon for heavy metal removal form aqueous solutions. *International Journal for Scientific Research & Development* 2025; **12(12)**, 63-67.

[12] Y Xu, Y Qu, Y Yang, B Qu, R Shan, H Yuan and Y Sun. Study of efficient adsorption mechanism of Pb^{2+} by magnetic coconut biochar. *International Journal of Molecular Sciences* 2022; **23(22)**, 14053.

[13] L Ni'mah, Mahfud and SR Juliastuti. Study of activated carbon from coconut shell waste to adsorb Cu and Mn metals in acid mine drainage. *Journal of Fibers and Polymers Composites* 2022; **1(1)**, 34-42.

[14] N Wahab, M Saeed, M Ibrahim, A Munir, M Saleem, M Zahra and A Waseem. Synthesis, Characterization, and applications of silk/bentonite clay composite for heavy metal removal from aqueous solution. *Frontiers in Chemistry* 2019; **7**, 00654.

[15] PN Daigboya, BIO Owolabi, FM Mtunzi and KO Adebowale. Clay-carbonaceous material composites: Towards a new class of functional adsorbents for water treatment. *Surfaces and Interfaces* 2020; **19**, 100506.

[16] SM Abegunde, KS Idowu, OM Adejuwon and T Adeyemi-Adejolu. A review on the influence of chemical modification on the performance of adsorbents. *Resources, Environment and Sustainability* 2020; **1**, 100001.

[17] R Ghibate, M Chrachmy, M Kerrou, M Ben Baaziz, M Alaqarbeh, A Amechrouq, R Taouil and O Senhaji. Eco-friendly adsorption of rhodamine B dye using punica granatum peel from an aqueous medium. *Green Analytical Chemistry* 2025; **12**, 100201.

[18] NB Allou, MA Tigori, AA Koffi, M Halidou, NS Eroi, P Atheba and A Trokourey. Methylene blue magnetic adsorption separation process from aqueous solution using corn cob. *Scientific African* 2023; **21**, e01828.

[19] J Serafin and B Dziejarski. Application of isotherms models and error functions in activated carbon CO_2 adsorption process. *Microporous and Mesoporous Materials* 2023; **354**, 112513.

[20] SM Mahgoub, MR Mahmoud, SHM Hafez, AA Allam, HE Alfassam, EE Abdel-Hady, AAA Anwar and R Mahmoud. Green chemistry approach for the removal of delafloxacin from aqueous solutions using calcinated layered double hydroxide: Adsorption mechanism and material

characterization. *Scientific African* 2025; **27**, e02535.

[21] M Kerrou, S Raada, D Mrani and A Elanssari. A comparative study of the adsorption of a cationic dye on three substrates. *Desalination and Water Treatment* 2023; **311**, 135-143.

[22] T Koroleva, B Pokidko, I Morozov, A Nesterenko, S Kortunkova, M Chernov, D Ksenofontov and V Krupskaya. Hydrothermal synthesis of kaolinite group minerals. *Materials* 2025; **18(3)**, 472.

[23] BM Saeed and MB Abdul-Kareem. Preparation and performance of a modified Iraqi red kaolin clay-based sorbent for methylene blue removal in acidic and basic solutions. *International Journal of Design and Nature Ecodynamics* 2025; **20(2)**, 241-249.

[24] M El-Habacha, A Dabagh, S Lagdali, Y Miyah, G Mahmoudy, F Sinan, M Chiban, S Iaich and M Zerbet. An efficient and adsorption of methylene blue dye on a natural clay surface: Modeling and equilibrium studies. *Environmental Science and Pollution Research* 2023; **31(53)**, 62065-62079.

[25] K Kalpana, S Arivoli and K Veeravelan. Activated carbon merremia emarginata adsorption capacities of low-cost adsorbent for removal of methylene blue. *Ecology Environment and Conservation* 2022; **22(08)**, S425-S430.

[26] CJ Hsu, YH Cheng, YP Huang, JD Atkinson and HC Hsi. A novel synthesis of sulfurized magnetic biochar for aqueous Hg(II) capture as a potential method for environmental remediation in water. *Science of the Total Environment* 2021; **784**, 147240.

[27] Darmadi, Mahidin, SS Azzahra and M Masrura. Adsorption of mercury(II) ion in aqueous solution by using bentonite-based monolith. *Key Engineering Materials* 2021; **885**, 77-84.

[28] HPI Indra, Darmadi, Adisalamun, A Chairunnisak and RCL Nasrullah. Removal of lead ion (Pb^{2+}) in water using modified clay-carbon-manganese monolith: Characterization and adsorption studies. *Elkawnie: Journal of Islamic Science and Technology* 2023; **9(2)**, 188-203.

[29] C Garcia-Carvajal, J Villaroel-Rocha, VCD Souza and K Sapag. Development of ceramic honeycomb monolith from natural zeolite tested as adsorbent to remove methylene blue in aqueous media. *Environmental Science and Pollution Research* 2022; **29**, 79890-79902.

[30] Activated carbon price kg powder, Available at: https://www.alibaba.com/showroom/activated-carbon-price-kg-pow¬der.html?utm_source= chatgpt.com, accessed September 2025.